Detailed electrical characterization of 200mm CMOS compatible GaN/Si HEMTs down to deep cryogenic temperatures

Donghyun Kim, C. Theodorou, A. Chanuel, Y. Gobil, M. Charles, E. Morvan, Jae Woo Lee, M. Mouis, G. Ghibaudo

Accepted to Solid State Electronics (2022)

Detailed electrical characterization of 200mm CMOS compatible GaN/Si HEMTs down to deep cryogenic temperatures

Donghyun Kim[1,3], C. Theodorou[1], A. Chanuel[2], Y. Gobil[2], M. Charles[2], E. Morvan[2], Jae Woo Lee[3], M. Mouis[1], G. Ghibaudo[1]

1) IMEP-LAHC, Univ. Grenoble Alpes, Minatec, 38016 Grenoble, France,

2) CEA-LETI, Univ. Grenoble Alpes, Minatec, 38054 Grenoble, France.

3) Department of Electronics and Information Engineering, Korea University, Sejeong Campus, South Korea.

Email: gerard.ghibaudo@minatec.grenoble-inp.fr, gerard.ghibaudo@gmail.com

Abstract

A detailed electrical characterization and transistor parameter extraction on 200mm CMOS compatible GaN/Si HEMTs was performed down to deep cryogenic temperatures. The main transistor parameters (threshold voltage V_{th}, low-field mobility μ_0, subthreshold swing SS, source-drain series resistance R_{sd}) were extracted in linear region using the Y-function and the Lambert-W function methods for gate lengths down to 0.1µm. The Y-function method was also employed in saturation region for the extraction of the saturation velocity. The results indicate that these GaN/Si HEMT devices demonstrate a very good functionality down to very low temperature with improvement of mobility and subthreshold slope. It was also shown by TLM analysis that the source-drain series resistance R_{sd} is more limited by the contact resistance than by the 2DEG access region resistance as temperature is lowered.

Keywords: GaN/Si, HEMT, transistor, parameter extraction, mobility, threshold voltage, access resistance, cryogenic temperature.

Author version – Published version available from Solid State Electronics, Vol. 197, no. 108448, 8 pp, doi: 10.1016/j.sse.2022.108448 (Nov. 2022). HAL reference: hal-03769945

1. Introduction

Cryogenic power electronics is a key enabling technology for various applications such as electromechanical drives, transportation, renewable systems and power networks [1-2]. It will bring higher power density, higher efficiency and superior performances due to higher operation speed, lower power dissipation stemming from reduced voltage, better switching characteristics, shorter transmission times due to lower metal resistance, increased integration density, better digital and analog device/circuit performances [1-2]. In this context, GaN HEMT technology has emerged as a promising candidate in cryogenic power electronics for high frequency and high power microwave applications due their high two dimensional electron gas (2DEG) mobility when operated at very low temperatures [3-9]. However, although several studies have already been reported about the cryogenic performances of GaN HEMT devices [10-13], there is still a lack of detailed analysis of the electronic properties of the channel and access regions under cryogenic operation.

Therefore, in this work, we present, for the first time, a complete electrical characterization of the transistor parameters (especially mobility, saturation velocity, threshold voltage, subthreshold swing, source-drain resistance…) as a function of gate length for 200mm CMOS compatible GaN/Si HEMTs operated down to deep cryogenic temperatures. We demonstrate that the 2DEG mobility is enhanced by phonon scattering reduction, and that the switching behaviour is considerably improved at very low temperatures. Moreover, we propose a TLM analysis of the source-drain series resistance, discriminating the contribution of contact and 2DEG access region resistances depending on temperature.

2. Experiments and methods

The HEMT devices under investigation belong to a GaN technology processed on 200 mm Silicon wafer designed for high frequency applications [14]. Figure 1 illustrates the device structure and cross section. The epitaxial stack was grown using metal organic vapor phase epitaxy (MOVPE) on a 200 mm high resistivity (111) silicon substrate. The structure consisted in transition layers and a 1.5 µm GaN carbon doped buffer layer followed by an AlGaN back barrier (300 nm) and a 150 nm unintentionally doped (UID) GaN channel. The back barrier is a patented structure consisting in a thin 10nm AlGaN 30% on top of a AlGaN gradient. It is designed as a compromise between good confinement efficiency and low thermal resistance [15]. An AlN spacer (1 nm) and a thin $Al_{0.28}Ga_{0.72}N$ (7 nm) layer formed the barrier. A capping layer of 10 nm SiN was used for passivation. Ohmic contact formation began with passivation and AlGaN barrier etching before Ti/Al deposition, chemical mechanical polishing (CMP) and annealing at 590 °C. Gate feet were patterned by ebeam lithography followed by passivation etching, TiN/W deposition and CMP. The gate head was formed

Author version – Published version available from Solid State Electronics, Vol. 197, no. 108448, 8 pp, doi: 10.1016/j.sse.2022.108448 (Nov. 2022). HAL reference: hal-03769945

by Ti/TiN/Al/TiN deposition and dry etching. Finally, vias were opened through the SiO_2 passivation and 1.4 µm Al deposition followed by lithography and dry etching formed the first level of interconnection. The test structure device gate length varied between L_g= 0.1µm and 3µm, the source-gate length L_{gs}=1µm or 5.5µm, the drain-gate length L_{gd}=1.5µm or 5.5µm. The device gate width was W_g=100µm or 125µm.

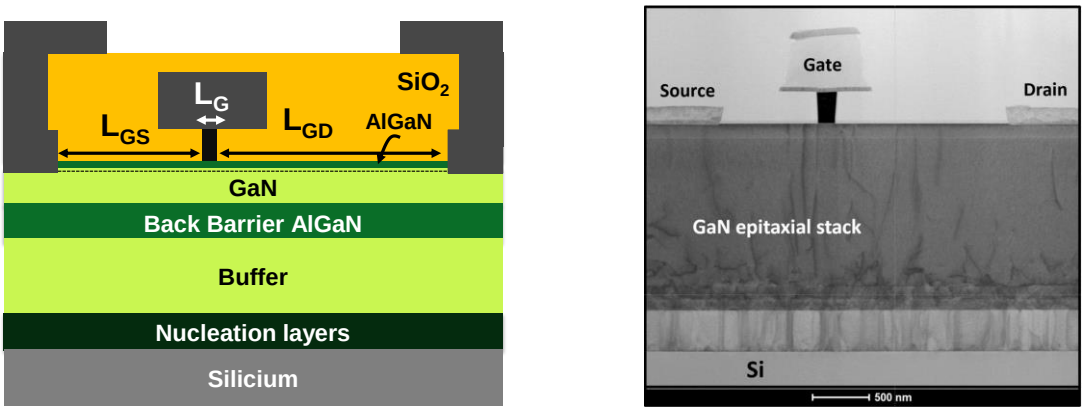

a) b)

Figure 1. Schematic of the epitaxial stack and TEM cross section of GaN/Si HEMTs**.**

The I_d-V_g transfer characteristics were measured in linear (V_d=50mV) and saturation (V_d=5V) regions using an HP 4156B semiconductor parameter analyser. The gate-to-channel capacitance was measured at room temperature with an HP 4284 LCR meter at a frequency of 1MHz, providing here a maximum capacitance of about 0.9µF/cm^2 above threshold, which is equivalent to an AlGaN/AlN thickness of about 8nm. The cryogenic measurements were performed on a 200mm liquid helium Susstec cryo-probe station with temperature varying between 10K and 300K.

On one hand, the transistor parameter extraction was carried out using the Y-function method, originally developed for Si MOSFETs [16] and recently validated on MIS-HEMT GaN devices at 300K [17], which allows removing the influence of the source-drain series resistance. The Y-function is defined from drain current I_d and transconductance g_m by [16],

$$Y(V_g) = I_d/\sqrt{g_m} \approx \sqrt{\frac{W_g}{L_g}.C_{ox}.\mu_0.V_d.(V_g - V_{th})}\,, \quad (1)$$

where C_{ox} is the maximum gate-to-channel capacitance associated to the coupling capacitance between the metal gate and GaN 2DEG through the AlGaN layer, μ_0 is the low field mobility and V_{th} the threshold voltage. The source-drain series resistance R_{sd} is then extracted, in linear operation, from the plateau of the quantity defined below plotted in strong inversion,

$$R_{sd} = \frac{V_d}{I_d} - \frac{L_g}{W_g.C_{ox}.\mu_0.(V_g - V_{th})}. \quad (2)$$

Author version – Published version available from Solid State Electronics, Vol. 197, no. 108448, 8 pp, doi: 10.1016/j.sse.2022.108448 (Nov. 2022). HAL reference: hal-03769945

On the other hand, the transistor parameter extraction was performed using the Lambert-W function modelling approach developed for Si MOS transistors at 300K [18] and recently extended at cryogenic temperatures [19]. In this case, the drain current in linear region including the R_{sd} influence is given by,

$$I_d = \frac{\frac{W_g}{L_g}\mu_0.Q_i.V_d}{1+R_{sd}.\frac{W_g}{L_g}\mu_0.Q_i}. \quad (3)$$

where the inversion charge Q_i is modelled from weak to strong inversion as,

$$Q_i = C_{ox}.\frac{n.kT}{q}.LW(e^{\frac{V_g-V_{th}}{n.kT/q}}), \quad (4)$$

where kT/q is the thermal voltage, n the subthreshold ideality factor and LW is the Lambert-W function [18]. This LW method presents the advantage to extract the MOSFET parameters over the full gate voltage range below and above threshold.

Finally, the Y-function method was applied in the saturation region for the extraction of the carrier saturation velocity v_{sat} as was originally demonstrated in Si MOSFETs [20]. In this case, Eq. (1) is used to extract the mobility degraded by the longitudinal electric field V_d/L_g, $\mu_{0d}=\mu_0/(1+\mu_0 V_d/(v_{sat}L_g))$, from the slope of the linear trend of Y(Vg) characteristics measured in saturation, such that the saturation velocity can be obtained from [20],

$$v_{sat} = \frac{\mu_0 V_d}{L_g\left(\frac{\mu_0}{\mu_{0d}}-1\right)}. \quad (5)$$

For comparison purpose, the saturation velocity was also extracted using the standard method based on the saturation drain current I_{dsat} and inversion charge at source terminal given by [20],

$$v_{sat} = \frac{I_{dsat}}{W_g.C_{ox}.(V_g-V_{th}-R_s.I_{dsat})}, \quad (6)$$

where R_s is the source series resistance.

3. Results and discussion

3.1. Transfer characteristics

Typical drain and source current transfer characteristics I_d-V_g and I_s-V_g measured in the linear region (V_d=50mV) are shown in Fig. 2. They were obtained on GaN HEMT devices with a gate length of L_g=150nm at various temperatures (10K-300K). As can be seen from the figure, there was a strong gate current I_g for high gate voltage in such Schottky gate devices. Indeed, drain current I_d strongly differed from source current I_s for V_g>1.5V. For this reason, the transistor parameter extraction was restricted to V_g up to 1V in order to avoid any gate leakage influence. Nonetheless, note that the I_d-V_g curves exhibited a very good behaviour below threshold as the temperature was lowered with an improved subthreshold slope, specific of cryogenic operation. Note also that the I_d-V_g curves were

Author version – Published version available from Solid State Electronics, Vol. 197, no. 108448, 8 pp, doi: 10.1016/j.sse.2022.108448 (Nov. 2022). HAL reference: hal-03769945

saturating well above threshold due to the strong impact of the series resistance effect caused by the contact and access regions as will be discussed below.

The corresponding transconductance g_m-V_g and Y-function Y-V_g characteristics up to V_g=1V are shown in Fig. 3, illustrating the increase of the maximum transconductance with temperature lowering and the linear behaviour of Y-function well above threshold.

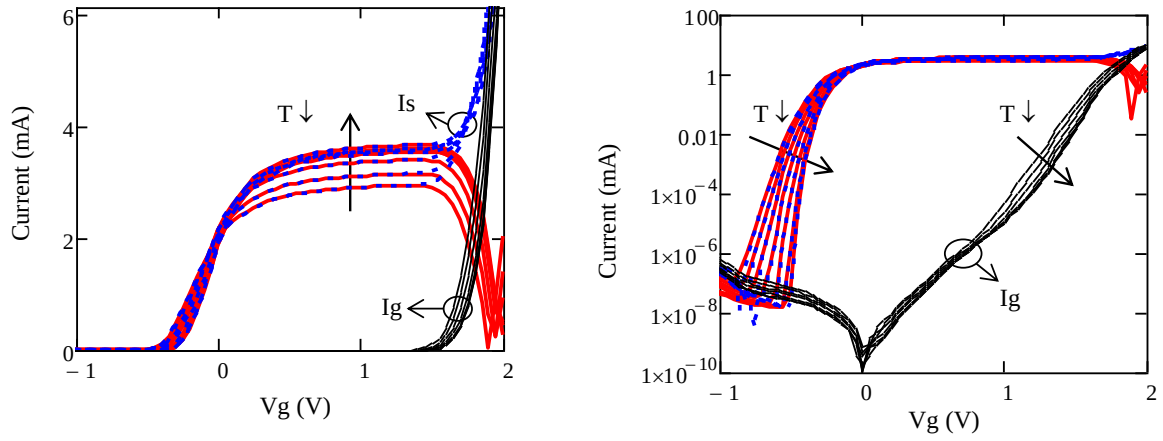

a) b)

Figure 2. Typical I_d-V_g characteristics in linear (a) and log (b) scale as obtained on GaN/Si HEMT devices for various temperatures T(K)=10, 50, 100, 150, 200, 250, 300 (V_d=50mV, L_g=150nm, L_{gs}=1µm, L_{gd}=1.5µm, W_g=100µm).

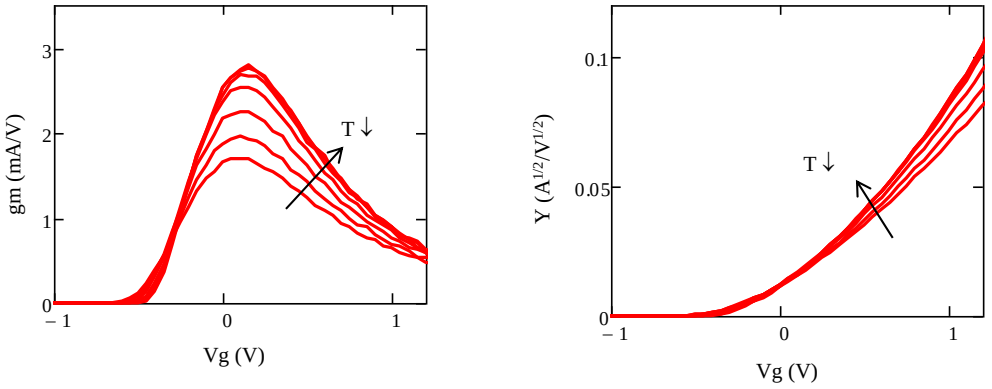

a) b)

Figure 3. Typical g_m-V_g (a) and Y-V_g (b) characteristics as obtained on GaN/Si HEMT devices with various temperatures T(K)=10, 50, 100, 150, 200, 250, 300 (V_d=50mV, L_g=3000nm, L_{gs}=1µm, L_{gd}=1.5µm, W_g=100µm).

3.2. Y-function based transistor parameter extraction

Author version – Published version available from Solid State Electronics, Vol. 197, no. 108448, 8 pp, doi: 10.1016/j.sse.2022.108448 (Nov. 2022). HAL reference: hal-03769945

Based on Eq. (1), the threshold V_{th} and low field mobility μ_0 were extracted respectively from the x-axis intercept and slope of the Y-function linear trends above threshold [16], for each gate length and temperature. Figure 4 shows the variations with temperature of the obtained threshold voltage V_{th} and low field mobility μ_0 for various gate lengths. As expected from cryogenic operation, one observes a linear increase of V_{th} with temperature lowering due to the evolution from Boltzmann to Fermi-Dirac carrier statistics as is usual in Si MOS transistors [21]. Note also that the V_{th} roll-off versus gate length was nearly independent of temperature, as mainly arising from electrostatic-induced short channel effect as is usually observed in Si MOSFETs [21]. Moreover, the low field mobility μ_0 was also increasing with temperature reduction due to phonon scattering diminution, especially for long channel devices, where μ_0 improved from 2000 $cm^2V^{-1}s^{-1}$ up to 4000 $cm^2V^{-1}s^{-1}$ for long channel, e.g. L_g=3000nm. It should be mentioned that these mobility values are in good agreement with literature results obtained on GaN HEMTs by Hall effect or transistor parameter extraction [10, 22], pointing out the good quality of our GaN/Si technological process. In Fig. 4(b) are also reported, for comparison purpose, the variations with temperature of the maximum field effect mobility deduced from the maximum transconductance and defined as $\mu_{femax}=g_{mmax}.L_g/(W_g.C_{ox}.V_d)$ [23], clearly revealing the huge underestimation of the mobility values obtained using this method, which is indeed inappropriate in the presence of large R_{sd} effect [24].

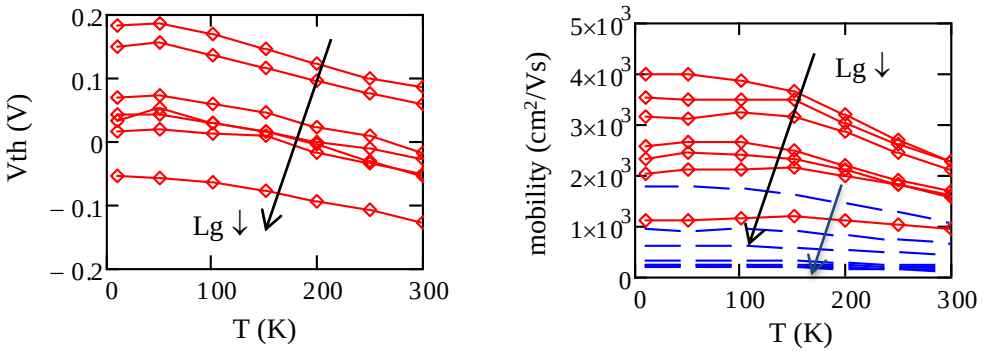

a) b)

Figure 4. Variations with temperature of a) threshold voltage V_{th} and b) electron low field mobility μ_0 (red solid line) and μ_{femax} (blue dashed lines) as obtained on GaN/Si HEMT devices with various gate lengths L_g(nm)= 100, 120, 150, 200, 500, 1000 and 3000 (V_d=50mV, L_{gs}=1µm, L_{gd}=1.5µm, W_g=100µm).

As can also be seen from Fig. 4, the low field mobility μ_0 was significantly reduced as the gate length was decreased. This is better illustrated in Fig. 5(a) where μ_0 has been plotted versus gate

Author version – Published version available from Solid State Electronics, Vol. 197, no. 108448, 8 pp, doi: 10.1016/j.sse.2022.108448 (Nov. 2022). HAL reference: hal-03769945

length for various temperatures. It clearly appears that the low field mobility for short channel is much less temperature dependent than for long channels, revealing a clear change in scattering mechanism as reducing the gate length. Indeed, in long channels, μ_0 is likely dominated by phonon scattering explaining the mobility increase at lower T. Instead, in short channels, μ_0 is almost constant with temperature, which is indicative of neutral scattering domination as was observed in scaled Si MOSFETs [19]. Therefore, these low field mobility data versus temperature and gate length were tentatively modelled using the same approach employed in Si MOSFET, where the mobility can be described as [19],

$$\mu_{0,mod} = \left[\frac{1}{\mu_{ph}}.\left(\frac{T}{300}\right)^{\alpha} + \frac{1}{\mu_N}.\left(1+\frac{L_c}{L_g}\right)^{\beta}\right]^{-1} \quad (7)$$

where μ_{ph} is the phonon-limited mobility at room temperature, μ_N is the temperature independent neutral defect-limited mobility for long channel, L_c being a critical gate length and α and β fitting parameters. As can be seen from Fig. 5, the simple model of Eq. (7) provided a good description of mobility variations both with gate length and with temperature. It clearly shows that the mobility degradation in short channel GaN HEMTs is also well interpreted by an increased contribution of neutral scattering defects. The latter ones should be mostly localized close to source-drain gate edges and could stem from the metal gate etching process.

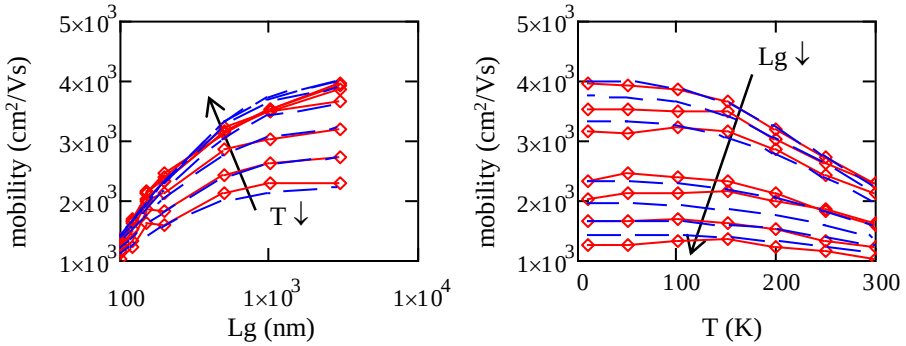

Figure 5. a) Experimental (red solid lines) and Eq. (7) modeled (blue dashed lines) variations of electron low field mobility μ_0 with gate length L_g for various temperatures T(K)=10, 50, 100, 150, 200, 250, 300 and b) variations of low field mobility μ_0 with temperature T for various gate lengths L_g(nm)= 100, 120, 150, 200, 500, 1000 and 3000 as obtained on GaN/Si HEMT devices (V_d=50mV, L_{gs}=1µm, L_{gd}=1.5µm, W_g=50µm). Model parameters: μ_{ph}=5000cm^2/Vs, μ_N=4100cm^2/Vs, L_c=160nm, α=3, β=1.3.

The variations with temperature of the subthreshold swing SS=dV_g/dlog(I_d) are shown in Fig. 6(a) for various gate lengths. As expected from cryo-operation, the subthreshold swing SS mostly followed

Author version – Published version available from Solid State Electronics, Vol. 197, no. 108448, 8 pp, doi: 10.1016/j.sse.2022.108448 (Nov. 2022). HAL reference: hal-03769945

the Boltzmann linear trend vs temperature over 100K before saturating at low temperature, likely due to some specific interface trap energy profile and/or to charge-induced-disorder potential fluctuations, as found in Si MOS devices [25, 26].

The access series resistance R_{sd} was extracted using Eq. (2) at strong inversion where its impact is maximized. The variations with temperature of the series resistance R_{sd} for various gate lengths are shown in Fig. 6(b). The access resistance R_{sd} values ranged typically around ≈1400 Ω.µm and increased linearly with temperature above 100K, whatever the gate length, emphasizing the R_{sd} extraction consistency against L_g. These $R_{sd}(T)$ variations are in line with the metallic degenerate behaviour observed for the sheet resistance of AlGaN/AlN/GaN HEMT structures with ≈10^{13}q/cm^2 2DEG carrier density [22, 27]. These variations will be discussed in more details below.

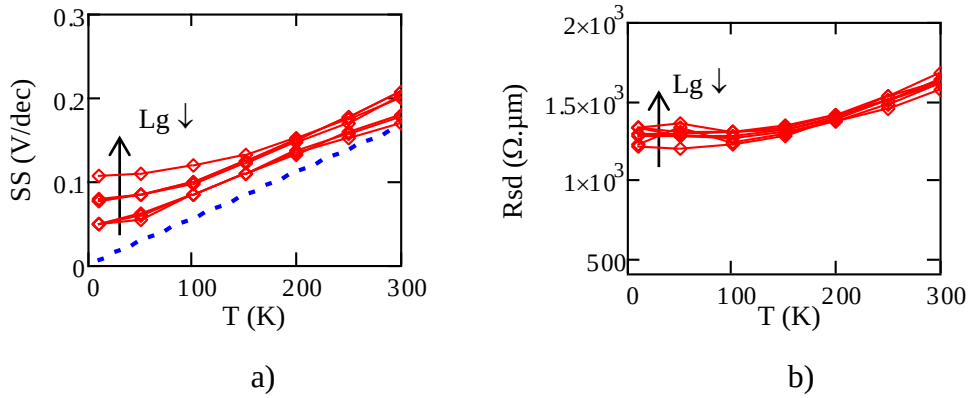

Figure 6. Typical variations with temperature of subthreshold swing SS (a) and access series resistance R_{sd} (b) as obtained on GaN/Si HEMT devices for various gate lengths L_g (nm)= 100, 120, 150, 200, 500, 1000 and 3000 (V_d=50mV, L_{gs}=1µm, L_{gd}=1.5µm, W_g=100µm).

3.3. Lambert-W-function based transistor parameter extraction

Lambert W function-based transistor parameter extractions were carried out using Levenberg-Marquardt procedure based on Eqs (3)-(4). Typical fits of the transfer characteristics obtained by LW function modelling, with optimized parameters (V_{th}, μ_0, n, R_{sd}), are illustrated in Fig. 7 over a wide gate voltage range from below to above threshold. Note that excellent fits of the characteristics can be obtained, especially around and above threshold i.e. V_g>-0.25V, for both $I_d(V_g)$, $g_m(V_g)$ and $Y(V_g)$ curves.

Author version – Published version available from Solid State Electronics, Vol. 197, no. 108448, 8 pp, doi: 10.1016/j.sse.2022.108448 (Nov. 2022). HAL reference: hal-03769945

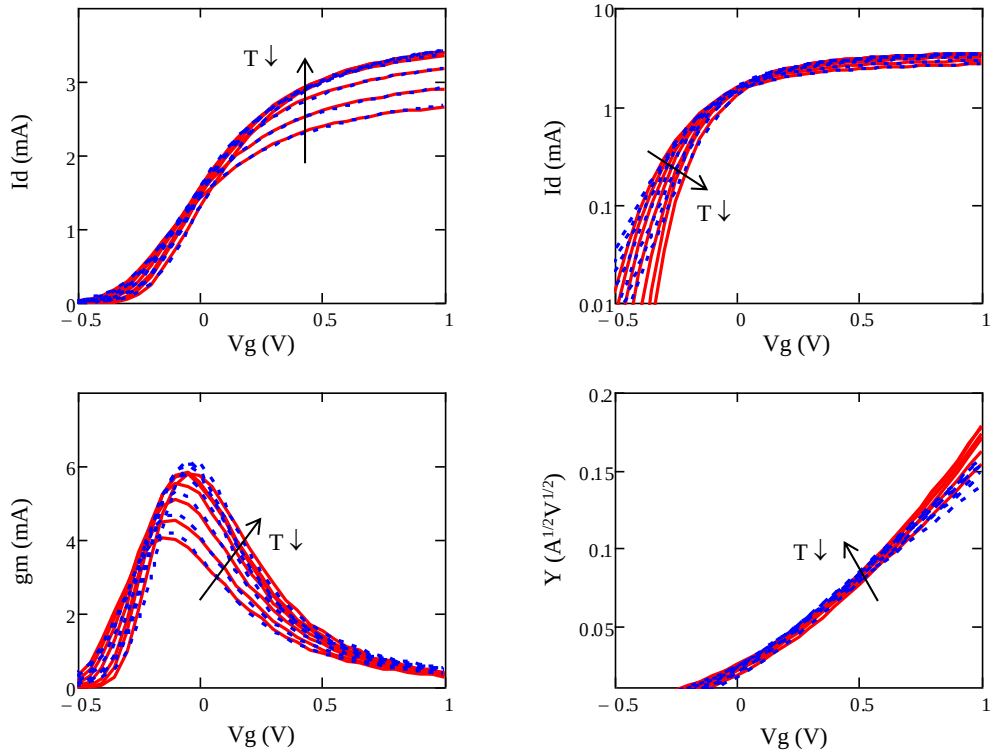

Figure 7. Experimental (red solid lines) and Lambert-W model fits (blue dashed lines) of the $I_d(V_g)$, $g_m(V_g)$ and $Y(V_g)$ characteristics for various temperatures T(K)= 10, 50, 100, 150, 200, 250 and 300 as obtained on GaN/Si HEMT devices (V_d=50mV, L_g=500nm, L_{gs}=1µm, L_{gd}=1.5µm, W_g=100µm).

In Fig. 8 are shown the variations with temperature of the threshold voltage V_{th} and of the low field mobility μ_0 obtained with the LW function fitting method (red solid lines) for devices with various gate lengths. For comparison purpose, the $V_{th}(T)$ and $\mu_0(T)$ curves extracted with Y-function method (blue dashed lines) are also reminded. Although slightly different, the V_{th} and μ_0 parameters extracted by both methods displayed the same behaviour with temperature and gate length, which was also observed in Si MOS devices [18, 19]. The good mobility values obtained by the LW function method again confirmed the quality of such GaN/Si HEMT devices.

In Fig. 9 are reported the variations with temperature and reciprocal temperature of the subthreshold ideality factor n_L obtained from the LW function fittings for various gate lengths (red solid lines). The ideality factor values directly deduced from the subthreshold swing SS (see Fig. 6a), n_{SS}=SS/(2.3×kT), are also reported in blue dashed lines. As can be seen, the LW function fitting procedure tended to overestimate the ideality factor, especially at low temperature. However, this inconvenience does not alter the validity of the transistor parameter extraction just below and above threshold. It should also be noticed that the 1/T dependence of the ideality factor has been previously found in Si MOSFETs and can be explained by the SS plateauing behaviour at low temperature [19].

Author version – Published version available from Solid State Electronics, Vol. 197, no. 108448, 8 pp, doi: 10.1016/j.sse.2022.108448 (Nov. 2022). HAL reference: hal-03769945

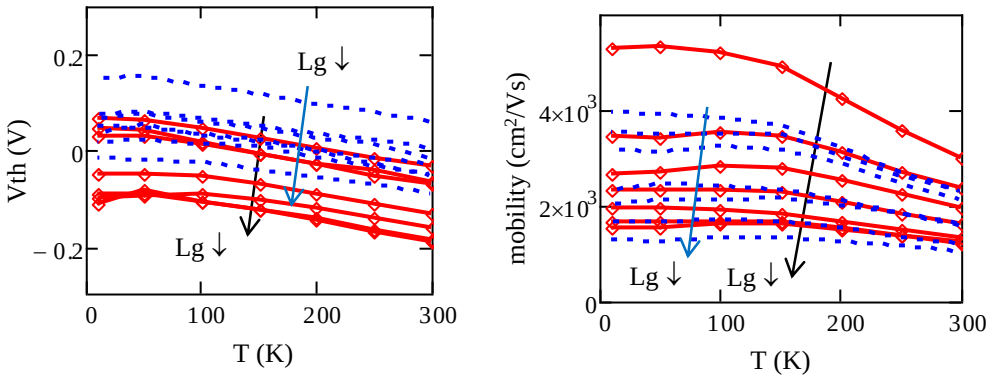

a) b)

Figure 8. Variations with temperature of a) threshold voltage V_{th} and b) electron low field mobility μ_0, as obtained from LW function extraction (red solid line) and from Y-function method extraction (blue dashed lines) on GaN/Si HEMT devices with various gate lengths L_g(nm)= 100, 120, 150, 200, 500, 1000 and 3000 (V_d=50mV, L_{gs}=1µm, L_{gd}=1.5µm, W_g=100µm).

The access series resistance values R_{sd} extracted by the LW function fitting method (red solid lines) are displayed in Fig. 10(a) along with those obtained by Y-function method (blue dashed lines) for a transistor with an access region distance $L_{sd}=L_{gs}+L_{gd}$=2.5µm, emphasizing the consistency of the two extraction methodologies. In Fig. 10(b), are reported the temperature dependence of the source and drain resistance R_{sd} extracted from Y-function method for two access region distances L_{sd1}= 2.5µm and L_{sd2}=11µm for various gate lengths. In this case, a larger temperature dependence of R_{sd} can be noticed for the devices with the longer access region distance.

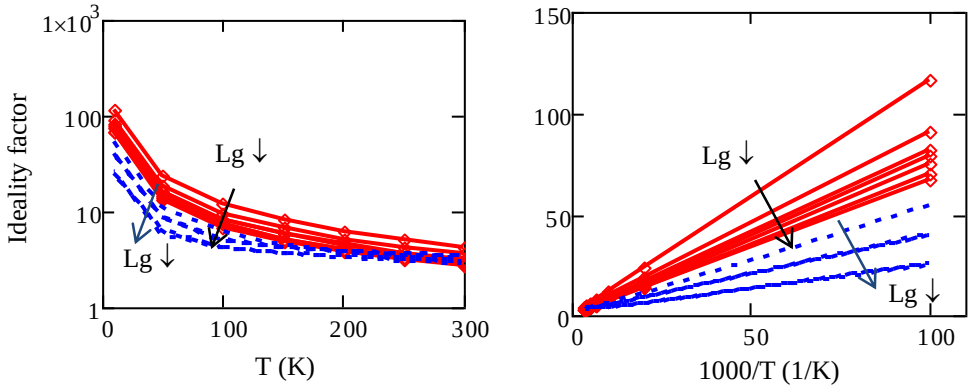

(a) (b)

Figure 9. Variations of subthreshold ideality factors n_L (red solid lines) and n_{SS} (blues dashed lines) and b) with temperature (a) and reciprocal temperature (b) as obtained on GaN/Si HEMT devices for various gate lengths L_g(nm)= 100, 120, 150, 200, 500, 1000 and 3000 (V_d=50mV, L_{gs}=1µm, L_{gd}=1.5µm, W_g=100µm).

Author version – Published version available from Solid State Electronics, Vol. 197, no. 108448, 8 pp, doi: 10.1016/j.sse.2022.108448 (Nov. 2022). HAL reference: hal-03769945

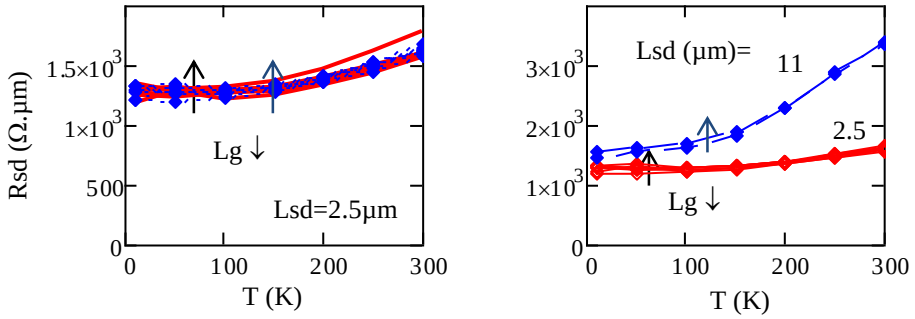

Figure 10. a) Variations with temperature of series resistance values R_{sd} extracted by LW function method (red solid lines) and by Y-function method (blue dashed lines) as obtained on GaN/Si HEMT devices for various gate lengths L_g(nm)= 100, 120, 150, 200, 500, 1000 and 3000 (V_d=50mV, L_{gs}=1µm, L_{gd}=1.5µm, W_g=100µm). b) Variations with temperature of series resistance values R_{sd} extracted by Y-function method for two access region distances L_{sd}=2.5µm and 11µm as obtained on GaN/Si HEMT devices for various gate lengths L_g(nm)= 1000 and 5000 (V_d=50mV, L_{gs}=5.5µm, L_{gd}=5.5µm, W_g=125µm).

In order to discriminate the contribution brought by the contact resistance R_c and by the 2DEG access region resistance $\rho_{2DEG}.L_{sd}$, ρ_{2DEG} being the 2DEG sheet resistance, a TLM analysis of the source-drain series resistance R_{sd} for two L_{sd} values was carried out using Eq. (8),

$$R_{sd}(L_{sd}) = 2.R_c + \rho_{2DEG}.L_{sd} \qquad (\Omega.\mu m). \tag{8}$$

By this way, ρ_{2DEG} and R_c can be obtained from,

$$\rho_{2DEG} = \frac{R_{sd}(L_{sd2}) - R_{sd}(L_{sd1})}{L_{sd2} - L_{sd1}} \tag{9a}$$

$$R_c = \frac{R_{sd}(L_{sd1}) - \rho_{2DEG}.L_{sd1}}{2} = \frac{R_{sd}(L_{sd2}) - \rho_{2DEG}.L_{sd2}}{2}. \tag{9b}$$

In Fig. 11(a) are displayed the variations of the contact resistance R_c and the 2DEG sheet resistance ρ_{2DEG} as obtained from Fig. 10(b) data using Eqs (9) for L_{sd1}=2.5µm and L_{sd2}=11µm. As can be seen, the contact resistance R_c was rather temperature independent (≈550Ω.µm), which reveals a quasi-metallic behaviour. Instead, the 2DEG sheet resistance ρ_{2DEG} increases significantly with temperature, likely due to the mobility reduction with temperature increase, as observed for long channel mobility in Figs 8(b), associated to a constant polarization-induced 2DEG carrier density. Since, at room temperature, ρ_{2DEG}≈200Ω and μ_0≈2000cm^{2}V^{-1}s^{-1}, it follows that the 2DEG electron density in the access regions is about ≈1.5x10^{13}/cm^2, which, for some reason, is about ≈30% larger than the standard polarization-induced value for the AlGaN/GaN system as measured e.g. by Hall effect in devices from the same technology [27, 28]. In Fig. 11(b) are shown the variations with temperature of the percentage contribution of the 2DEG access region resistance to the total source-

Author version – Published version available from Solid State Electronics, Vol. 197, no. 108448, 8 pp, doi: 10.1016/j.sse.2022.108448 (Nov. 2022). HAL reference: hal-03769945

drain resistance $R_{sd}=2.R_c+\rho_{2DEG}.L_{sd}$. As can be seen, the contact resistance contribution is enhanced as the temperature is lowered and can reach up to 90% (resp. 70%) for an access region length L_{sd}=2.5µm (resp. 11µm).

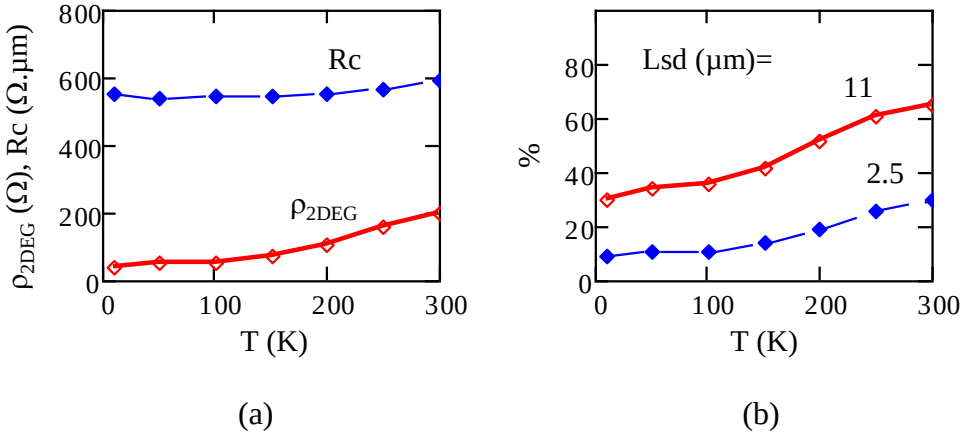

Figure 11. a) Variations with temperature of the 2DEG sheet resistance ρ_{2DEG} (red solid lines) and of contact resistance R_c (blue dashed lines) as obtained from R_{sd} TLM analysis on GaN/Si HEMT devices with various access region lengths L_{sd}=2.5 and 11 µm. b) Variations with temperature of percentage contribution of 2DEG access region resistance to the total source-drain resistance R_{sd} for two access region distances L_{sd}=2.5µm and L_{sd}=11µm as obtained from Fig. 10(b) data.

Finally, the saturation velocity v_{sat} was extracted using the Y-function (Eq. (5)) and standard (Eq. (6)) methods after having recorded the $I_d(V_g)$ characteristics in saturation region (V_d=5V, not shown here). In Fig. 12(a) are reported the variations with temperature of such extracted saturation velocities for various gate lengths. It should be mentioned that the value of the source resistance R_s needed in Eq. (6) was taken, according to Ohm's law, as a portion of the total resistance R_{sd} such as $R_s=R_c+L_{gs}.\rho_{2DEG}$. As can be seen from Fig. 12(a), the v_{sat} values obtained by the standard method (Eq. (6)) were significantly underestimated with respect to those deduced from Y-function, especially when the R_s correction was overlooked (R_s=0 in Eq. (6)) for short channels. It should be noted that the overall temperature dependence of v_{sat} is in agreement with those obtained on Si MOS transistors [21]. In Fig. 12(b) are shown the corresponding variations of v_{sat} with gate length, revealing as is usual the increase of v_{sat} with channel length reduction, which is inherent to the extraction procedure and/or velocity overshoot effect [20, 21]. It is worth noting that these saturation velocity values, found around 10^7cm/s, are in good agreement with those previously reported in GaN HEMTs [29-33].

Author version – Published version available from Solid State Electronics, Vol. 197, no. 108448, 8 pp, doi: 10.1016/j.sse.2022.108448 (Nov. 2022). HAL reference: hal-03769945

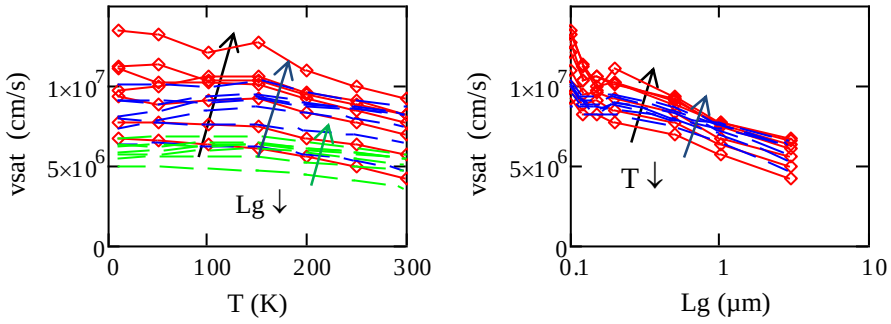

Figure 12. a) Variations with temperature of saturation velocity v_{sat} as extracted from Y-function (Eq. (5), red solid lines), or using the standard method with (blue dashed lines) or without (green dashed lines) R_{sd} correction (Eq. (6)), as obtained for various gate lengths L_g(nm)= 100, 120, 150, 200, 500, 1000 and 3000 (V_g=1.5V, V_d=5V & V_d=50mV, W_g=100µm). b) Variations with gate length of saturation velocity v_{sat} as extracted from Y-function (Eq. (5), red solid lines), or using the standard method (blue dashed lines) with R_s correction (Eq. (6)), as obtained on GaN/Si HEMT devices for various temperatures.

3. Summary and Conclusion

We carried out a detailed electrical characterization and a thorough transistor parameter extraction on 200mm CMOS-compatible GaN/Si HEMTs down to deep cryogenic temperatures. The main transistor parameters (threshold voltage V_{th}, low-field mobility μ_0, and subthreshold swing, SS, source-drain series resistance R_{sd}) were extracted in linear region (V_d=50mV) using Y-function and Lambert-W function methods for gate lengths from 3µm down to 0.1µm. The Y-function method was also employed in saturation region (V_d=5V) for the extraction of the saturation velocity. The results indicate that those 200mm CMOS-compatible GaN/Si HEMT devices display very good functionality down to very low temperature (10K), with significant improvement of mobility and subthreshold slope. In long channels, the low field mobility μ_0 was found to increase from 2000 $cm^2V^{-1}s^{-1}$ up to 4000 $cm^2V^{-1}s^{-1}$ from 300K down to 10K due to phonon scattering reduction. In contrast, in short devices, the low field mobility was nearly temperature independent, likely due to neutral defect scattering dominance. The saturation velocity v_{sat} was found to exceed 10^7cm/s at low temperature. The source-drain series resistance R_{sd} was shown, by TLM analysis, to be more controlled by the contact resistance R_c than by the 2DEG access region resistance as temperature was decreased. Finally, it is worth noting that the Lambert-W function modelling of the drain current characteristics,

Author version – Published version available from Solid State Electronics, Vol. 197, no. 108448, 8 pp, doi: 10.1016/j.sse.2022.108448 (Nov. 2022). HAL reference: hal-03769945

which has demonstrated its power in the case in Si MOSFETs [19], could provide a simple compact model for such GaN/Si HEMTs operation, down to deep cryogenic conditions.

Acknowledgment

This work was partially supported by EU H2020 RIA project SEQUENCE (Grant No. 871764. This work received funding from the ECSEL Joint Undertaking (JU) under grant agreement No 783274, project 5G GaN2. The JU receives support from the European Union's Horizon 2020 research and innovation program and France, Germany, Slovakia, Netherlands, Sweden, Italy, Luxembourg, Ireland. This work was also partly supported by the French Armed Forces Ministry through the "Agence Innovation Défense".

Author version – Published version available from Solid State Electronics, Vol. 197, no. 108448, 8 pp, doi: 10.1016/j.sse.2022.108448 (Nov. 2022). HAL reference: hal-03769945

References

1. K. Rajashekara and B. Akin, "A review of cryogenic power electronics - status and applications," 2013 International Electric Machines & Drives Conference, 2013, pp. 899-904.
2. H. Gui et al, "Review of Power Electronics Components at Cryogenic Temperatures", IEEE Trans. on Power Electronics, 35, 5144-5156 (2020).
3. R. Ren et al., "Characterization of 650 V Enhancement-mode GaN HEMT at Cryogenic Temperatures," 2018 IEEE Energy Conversion Congress and Exposition (ECCE), 2018, pp. 891-897.
4. R. Ren et al., "Characterization and Failure Analysis of 650-V Enhancement-Mode GaN HEMT for Cryogenically Cooled Power Electronics," IEEE Journal of Emerging and Selected Topics in Power Electronics, 8, 66-76 (2020).
5. P. Kushwaha et al., "Characterization of GaN HEMT at Cryogenic Temperatures," 2021 IEEE MTT-S International Microwave and RF Conference (IMARC), 2021, pp. 1-4.
6. Y. Wei, M. M. Hossain and A. Mantooth, "Comprehensive Cryogenic Characterizations of a Commercial 650 V GaN HEMT," 2021 IEEE International Future Energy Electronics Conference (IFEEC), 2021, pp. 1-6.
7. J. Colmenares, et al, "Experimental characterization of enhancement mode gallium-nitride power field-effect transistors at cryogenic temperatures," 2016 IEEE 4th Workshop on Wide Bandgap Power Devices and Applications (WiPDA), 2016, pp. 129-134.
8. C.-H. Lin, et al. "Transient pulsed analysis on GaN HEMTs at cryogenic temperatures." IEEE electron device letters, 26, 710-712. (2005).
9. L. Nela, et al, "Performance of GaN Power Devices for Cryogenic Applications Down to 4.2 K," in IEEE Transactions on Power Electronics, 36, 7412-7416 (2021).
10. X. F. Zhang, et al, “Electrical characteristics of AlInN/GaN HEMTs under cryogenic operation,” Chin. Phys. B, 22, 017202 (2013).
11. D. Keum and H. Kim, "Low-temperature characteristics of normally-off AlGaN/GaN-on-Si gate-recessed MOSHFETs", Cryogenics, 93, 51-55 (2018).
12. A. Endoh, et al. "Cryogenic characteristics of sub- 100- nm- gate AlGaN/GaN MIS- HEMTs." physica status solidi (c), 5, 1917-1919. (2008).
13. A. Endoh, et al. "Effect of temperature on cryogenic characteristics of AlGaN/GaN MIS-HEMTs." physica status solidi (c), 6, . S964-S967 (2009).
14. A. Chanuel, et al, "Breakdown Mechanism of AlGaN/GaN HEMT on 200mm Silicon Substrate with Silicon Implant assisted Contacts", submitted to IEEE Trans. on Electron Devices (2022).

Author version – Published version available from Solid State Electronics, Vol. 197, no. 108448, 8 pp, doi: 10.1016/j.sse.2022.108448 (Nov. 2022). HAL reference: hal-03769945

15. J.C. Jacquet et al, "Field-effect transistor with optimised performance and gain", Patent n°EP3369115 A1 (2016).
16. G. Ghibaudo, "A new method for the extraction of MOSFET parameters", Electronics Letters, 24, 543-544 (1988).
17. R. Kom Kammeugne, et al, "Accurate Statistical Extraction of AlGaN/GaN HEMT Device Parameters Using the Y-function", Solid-State Electronics, 184, 108078 (2021).
18. T. A. Karatsori, et al, "Full gate voltage range Lambert-function based methodology for FDSOI MOSFET parameter extraction", Solid State Electronics, 111, 123-128 (2015).
19. F. Serra di Santa Maria, et al, "Lambert-W Function-based Parameter Extraction for FDSOI MOSFETs Down to Deep Cryogenic Temperatures", Solid-State Electronics, 186, 108175 (2021).
20. C. Diouf, et al, "Y function method applied to saturation regime: apparent saturation mobility and saturation velocity extraction", Solid State Electronics, 85, 12–14 (2013).
21. F. Balestra and G. Ghibaudo, "Device and Circuit Cryogenic Operation for Low Temperature Electronics". Kluwers, 2001.
22. E. Dogmus, et al. "InAlGaN/GaN HEMTs at cryogenic temperatures." Electronics, 5, 31 (2016).
23. S. C. Sun and J. D. Plummer, "Electron Mobility in Inversion and Accumulation Layers on Thermally Oxidized Silicon Surfaces," in IEEE Journal of Solid-State Circuits, 15, 4, 562-573 (1980).
24. B. Cabon-Till, G. Ghibaudo, and S. Cristoloveanu. "Influence of source-drain series resistance on MOSFET field-effect mobility", Electronics Letters, 21, 457-458 (1985).
25. H. Bohuslavskyi, et al, "Cryogenic Subthreshold Swing Saturation in FD-SOI MOSFETs described with Band Broadening", IEEE Electron Device Letters, 40, 784-787 (2019).
26. G. Ghibaudo, et al, "On the modelling of temperature dependence of subthreshold swing in MOSFETs down to cryogenic temperature", Solid-State Electronics, 170, 107820 (2020).
27. I. Nifa, et al. "Characterization of 2DEG in AlGaN/GaN heterostructure by Hall effect." Microelectronic Engineering, 178, 128-131 (2017).
28. J. Lehmann et al., "Influence of epitaxy and gate deposition process on Ron resistance of AlGaN/GaN-on-Si HEMT," 2015 IEEE 27th International Symposium on Power Semiconductor Devices & IC's (ISPSD), 2015, pp. 261-264.
29. S. Bajaj, et al. "Density-dependent electron transport and precise modeling of GaN high electron mobility transistors", Applied Physics Letters, 107, 153504 (2015).
30. C. H. Oxley, et al, "On the temperature and carrier density dependence of electron saturation velocity in an AlGaN/GaN HEMT," in IEEE Transactions on Electron Devices, 53, 565-567 (2006).

Author version – Published version available from Solid State Electronics, Vol. 197, no. 108448, 8 pp, doi: 10.1016/j.sse.2022.108448 (Nov. 2022). HAL reference: hal-03769945

31. C.H. Oxley, and M. J. Uren. "Measurements of unity gain cutoff frequency and saturation velocity of a GaN HEMT transistor", IEEE transactions on electron devices, 52, 165-169 (2005).
32. L. Ardaravicius, et al. "Electron drift velocity in AlGaN/GaN channel at high electric fields", Applied Physics Letters, 83, 4038-4040 (2003).
33. T. Fang, et al, "Effect of optical phonon scattering on the performance limits of ultrafast GaN transistors", In 69th IEEE Device Research Conference (pp. 273-274).

Author version – Published version available from Solid State Electronics, Vol. 197, no. 108448, 8 pp, doi: 10.1016/j.sse.2022.108448 (Nov. 2022). HAL reference: hal-03769945